Generalized stress intensity factors of V-shaped notch in a round bar under torsion, tension, and bending

Nao-Aki Noda [*], Yasushi Takase

Department of Mechanical Engineering, Kyushu Institute of Technology, 1-1, Sensui-cho, Tobata, Kitakyushu 804-8550, Japan

Abstract

In this study, generalized stress intensity factors K_{I,λ_1}, K_{II,λ_2}, and K_{III,λ_4} are calculated for a V-shaped notched round bar under tension, bending, and torsion using the singular integral equation of the body force method. The body force method is used to formulate the problem as a system of singular integral equations, where the unknown functions are the densities of body forces distributed in an infinite body. In order to analyze the problem accurately, the unknown functions are expressed as piecewise smooth functions using three types of fundamental densities and power series, where the fundamental densities are chosen to represent the symmetric stress singularity and the skew-symmetric stress singularity. Generalized stress intensity factors at the notch tip are systematically calculated for various shapes of V-shaped notches. Normalized stress intensity factors are given by using limiting solutions; they are almost determined by notch depth alone, and almost independent of other geometrical parameters. The accuracy of Benthem–Koiter's formula proposed for a circumferential crack is also examined through the comparison with the present analysis.
© 2002 Elsevier Science Ltd. All rights reserved.

Keywords: Elasticity; Body force method; Sharp notch; V-shaped notch; Tension; Bending; Torsion; Test specimen; Generalized stress intensity factor

1. Introduction

In this study generalized stress intensity factors K_{I,λ_1}, K_{II,λ_2}, K_{III,λ_4} are analyzed for a V-shaped notch in a round test specimens. As shown in Fig. 1, here, three types of loading at infinity will be considered; that is, under tension, bending, and torsion. First, the body force method is applied and the problem is expressed as singular integral equations. Then, the unknown functions are expressed as piecewise smooth functions using three types of fundamental densities and power series. Here the fundamental densities are chosen to represent the symmetric stress singularity, and the skew-symmetric stress singularity. Finally, generalized stress intensity factors at the notch tips are systematically calculated with varying opening angel of notch γ, inclination angle of notch β, and depth of notch $2t/D$ under three types of loadings.

---

[*] Corresponding author.
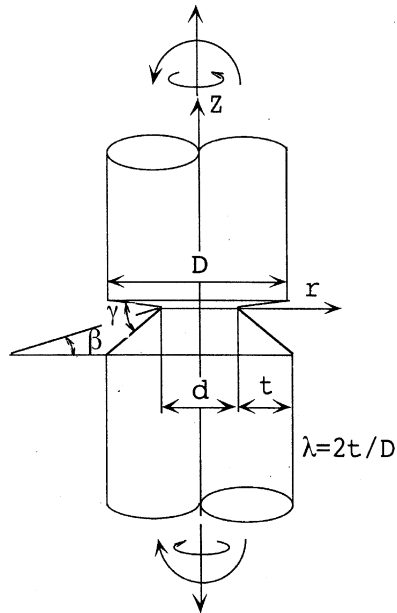*E-mail address:* noda@mech.kyutech.ac.jp (N.-A. Noda).

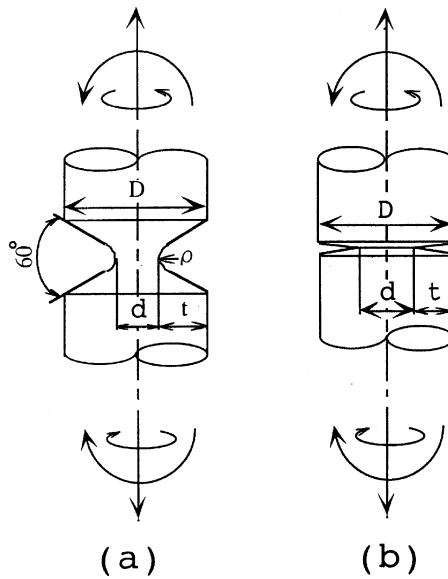Fig. 1. 60° V-shaped notched bar under tension, bending, and torsion.

Fig. 2. 60° V-shaped notched bar under tension, bending, and torsion: (a) case of notch root radius, (b) case of crack.

These solutions are useful especially in the following issues:

(1) When $\beta = \gamma = 0$ in Fig. 1, the problem is reduced to a circumferential crack in a round bar (see Fig. 2(a)), which has been used as a test specimen determining fracture toughness of materials. Although

Benthem–Koiter's formulas [1] have been often used to estimate the stress intensity factors, the accuracy has not been discussed until now except for tension case [2].

(2) When $\beta = 0°$, $\gamma = 60°$ in Fig. 1, the problem is reduced to the limiting solution when $\rho \to 0$ for fatigue test specimens in Fig. 2(b). Fatigue notch effects in metals have been often investigated using the specimen's geometry where ρ is the root radius of notches. Noda–Takase [3] proposed convenient formulas useful for evaluating any dimensions of notches within 1% error. However, the accuracy of the formulas should be confirmed by comparing with the exact solution when $\rho \to 0$. In the previous study the solution when $\rho \to 0$ was only estimated from the cases of very small radius of ρ because it was not available.

(3) The problem of Fig. 1 itself is important as a test specimen in considering the application of generalized stress intensity factors defined at corners of dissimilar materials as shown in the next sections in detail.

2. Singular stress fields at the corner of inclusion

Consider an inclusion corner as shown in Fig. 3. In the vicinity of notch tip in Fig. 1 two-dimensional state of stress can be assumed, which is corresponding to the case of $G_2 = 0$ in Fig. 3. It should be noted that the polar coordinate (r, θ) in Fig. 3 is different from the cylindrical coordinate (r, θ, z) in Fig. 1. In Fig. 3, the deformation around the corner tip can be separated into two parts; in-plane deformation and anti-plane deformation.

The in-plane deformation around the corner tip consists of mode I and mode II types, each having distinct singular index λ_1, λ_2. On the other hand, anti-plane mode III deformation has symmetric or skew-symmetric types of deformation alternatively, each having distinct singular index λ_3, or λ_4. Then, the singular stress field due to in-plane deformation is controlled by generalized stress intensity factors K_{I,λ_1}, K_{II,λ_2}, K_{III,λ_3}, K_{III,λ_4} as shown in the following equation [4–7]:

When $G_1 < G_2$,

$$\sigma_{ij} = \frac{K_{I,\lambda_1}}{r^{1-\lambda_1}} f_{ij}^{I}(\theta) + \frac{K_{II,\lambda_2}}{r^{1-\lambda_2}} f_{ij}^{II}(\theta) + \frac{K_{III,\lambda_3}}{r^{1-\lambda_3}} f_{ij}^{III,\lambda_3}(\theta) \tag{1}$$
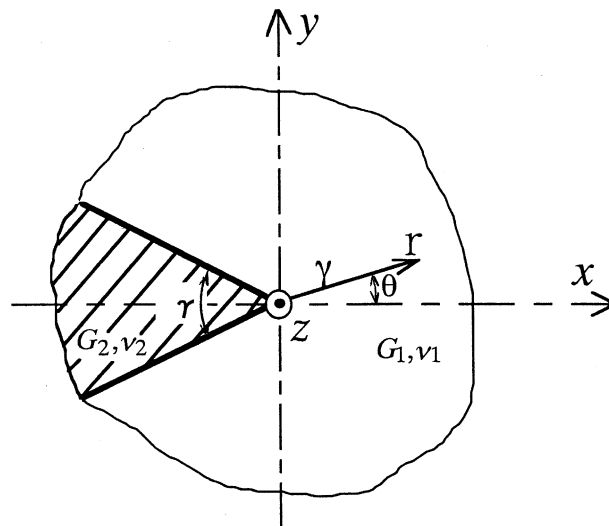

Fig. 3. Singular stress fields near a corner of jointed dissimilar materials under in-plane and anti-plane loads.

When $G_1 > G_2$,

$$\sigma_{ij} = \frac{K_{\mathrm{I},\lambda_1}}{r^{1-\lambda_1}} f_{ij}^{\mathrm{I}}(\theta) + \frac{K_{\mathrm{II},\lambda_2}}{r^{1-\lambda_2}} f_{ij}^{\mathrm{II}}(\theta) + \frac{K_{\mathrm{III},\lambda_4}}{r^{1-\lambda_4}} f_{ij}^{\mathrm{III},\lambda_4}(\theta) \tag{2}$$

Here, the singular stress field due to in-plane deformation consists of symmetric state of stress $1/r^{1-\lambda_1}$ and skew-symmetric state of stress $1/r^{1-\lambda_2}$. As an example, the singular stress σ_θ around the inclusion corner for material 1 can be expressed in the following form:

$$\begin{aligned} f_{\theta,1}^{\mathrm{I}}(\theta) = \frac{\lambda_1}{\sqrt{2\pi}(\alpha-\beta)} \langle [\lambda_1(\alpha-\beta)\sin\{\gamma-\lambda_1(\gamma-\pi)\} + (1-\beta)\sin(\lambda_1\pi)] \\ \times \cos\{(\lambda_1+1)\theta\} + [(\lambda_1+1)(\alpha-\beta)\sin\{\lambda_1(\gamma-\pi)\}] \times \cos\{(\lambda_1-1)\theta\}\rangle \end{aligned} \tag{3}$$

$$\begin{aligned} f_{\theta,1}^{\mathrm{II}}(\theta) = \frac{\lambda_2}{\sqrt{2\pi}(\alpha-\beta)} \langle [\lambda_2(\alpha-\beta)\sin\{\gamma-\lambda_2(\gamma-\pi)\} - (1-\beta)\sin(\lambda_2\pi)] \times \sin\{(\lambda_2+1)\theta\} \\ + [(\lambda_2+1)(\alpha-\beta)\sin\{\lambda_2(\gamma-\pi)\}] \times \sin\{(\lambda_2-1)\theta\}\rangle \end{aligned} \tag{4}$$

where

$$\alpha = \frac{G_2(\kappa_1+1) - G_1(\kappa_2+1)}{G_2(\kappa_1+1) + G_1(\kappa_2+1)}, \qquad \beta = \frac{G_2(\kappa_1-1) - G_1(\kappa_2-1)}{G_2(\kappa_1+1) + G_1(\kappa_2+1)} \tag{5}$$

$$\begin{aligned} \kappa_i &= \frac{(3-v_i)}{(1+v_i)} \quad \text{(for plane stress)} \\ \kappa_i &= (3-4v) \quad \text{(for plane strain)}, \ (i=1,2) \end{aligned} \tag{6}$$

The notation λ_1 and λ_2 are the minimum roots in the range $0 < \mathrm{Re}(\lambda) < 1$ of the following eigenequations [8]. When the combination of the two materials is such that $\beta(\alpha-\beta) > 0$, both λ_1 and λ_2 are real.

For mode I

$$\begin{aligned} D_1(\alpha,\beta,\gamma,\lambda) = (\alpha-\beta)^2\lambda^2(1-\cos 2\gamma) + 2\lambda(\alpha-\beta)\sin\gamma\{\sin\lambda\gamma + \sin(2\pi-\gamma)\} \\ + 2\lambda(\alpha-\beta)\beta\sin\gamma\{\sin\lambda(2\pi-\gamma) - \sin\lambda\gamma\} + (1-\alpha^2) - (1-\beta^2)\cos 2\lambda\pi \\ + (\alpha^2-\beta^2)\cos\{2\lambda(\gamma-\pi)\} = 0 \end{aligned} \tag{7}$$

For mode II

$$\begin{aligned} D_2(\alpha,\beta,\gamma,\lambda) = (\alpha-\beta)^2\lambda^2(1-\cos 2\gamma) + 2\lambda(\alpha-\beta)\sin\gamma\{\sin(2\pi-\gamma) + \sin\lambda\gamma\} \\ - 2\lambda(\alpha-\beta)\beta\sin\gamma\{\sin\lambda(2\pi-\gamma) - \sin\lambda\gamma\} + (1-\alpha^2) - (1-\beta^2)\cos 2\lambda\pi \\ + (\alpha^2-\beta^2)\cos\{2\lambda(\gamma-\pi)\} = 0 \end{aligned} \tag{8}$$

On the other hand, the singularity due to anti-plane deformation is determined by the root of the following eigenequations [5].

For a symmetric state of stress singularity

$$\frac{\sin\lambda(\gamma-\pi)}{\sin\lambda\pi} = +\frac{\Gamma+1}{\Gamma-1} \tag{9}$$

For a skew-symmetric state of stress singularity

$$\frac{\sin\lambda(\gamma-\pi)}{\sin\lambda\pi} = -\frac{\Gamma+1}{\Gamma-1} \tag{10}$$

where $\Gamma = G_2/G_1$. Denote the notation λ_3 as the root of Eq. (9), and the one λ_4 as the root of Eq. (10). When $G_2 > G_1$, there is a real root λ_3 of Eq. (1), but no roots λ_4 of Eq. (2). On the contrary, when $G_2 < G_1$, there is a real root λ_4 of Eq. (2), but no roots λ_3 of Eq. (1).

In notch problems as shown in Fig. 1 we can put $G_2 = 0$, $\alpha = -1$, and $\beta = -0.5$. Then, the values of λ_1, λ_2, λ_4 are given as the roots of the following characteristic equations:

$$\begin{aligned}
\text{mode I:} \quad & \sin[\lambda_1(2\pi - \gamma)] = -\lambda_1 \sin\gamma \\
\text{mode II:} \quad & \sin[\lambda_2(2\pi - \gamma)] = \lambda_2 \sin\gamma \\
\text{mode III:} \quad & \sin[\lambda_4(\pi - \gamma)] = \sin(\lambda_4\pi)
\end{aligned} \tag{11}$$

3. Difference between inclusion corners and ordinary cracks in terms of fracture mechanics

In the previous studies diamond-shaped inclusions [9–11], rectangular inclusions [3,6,7,12], a cylindrical inclusions [13] were analyzed. In those problems, the generalized stress intensity factors were obtained, and, therefore, the singular stresses can be expressed as Eqs. (1) and (2). However, if we want to evaluate fracture strength based on Eqs. (1) and (2), we have to consider the following issues different from cracks.

(A) The singular stress around inclusion corner consists of three different components, each having distinct singular index, $(\lambda_1, \lambda_2, \lambda_3)$ or $(\lambda_1, \lambda_2, \lambda_4)$. On the other hand, cracks always have the same singular index, that is, $\lambda_1 = \lambda_2 = \lambda_4 = 0.5$.

(B) Since fracture appears on the interface around the inclusion corner, the strength of bimaterial interface should be taken into account. On the other hand, for cracks only the strength of one material is in question.

The authors think (A) and (B) should be considered separately. Since sharp notches like Fig. 1 does not have interface, we can focus on discussing (A) if we use notched bar as a test specimen.

In our previous studies [14–16] we discuss the notch strength of acrylic resin using notched plate specimens [9].

4. Numerical solution of singular integral equations of body force method

In this section, by taking torsion problem as an example the method of analysis will be explained. Consider prospective boundaries for a notched bar in Fig. 4 in an infinite body, which has the same configuration of Fig. 1. On the idea of the body force method the problem is reduced to a singular integral equation (12), where unknowns are body force density distributed in the θ-direction along the prospective boundary for a notched bar.

$$-\frac{1}{2}F_\theta(s) + \int_L h_{n\theta}^{F_\theta}(l,s)F_\theta(l)\,\mathrm{d}l = -\tau_{n\theta}^\infty(s) \tag{12}$$

Here, $\int_L$ represents integrating the body forces on the imaginary boundary. The notation $\tau_{n\theta}^\infty(s)$ denotes a shear stress appearing at the point s due to torsional moment at infinity. The notation $h_{n\theta}^{F_\theta}(l,s)$ denotes a stress induced at the collocation point s when the body force with unit density F_θ is acting at the point l.

As shown in Fig. 5, around the notch tip the body forces are expressed as a combination of two types of distributions, that is, symmetric mode I, and skew-symmetric mode II types, to the bisector of the V-Shaped notch. In other words, along the region BAB′ in Fig. 4, the distributed body force densities are approximated as shown in Eq. (13) using power series $W_\theta^{\mathrm{III},\lambda_3}$, $W_\theta^{\mathrm{III},\lambda_4}$, and two types of fundamental density
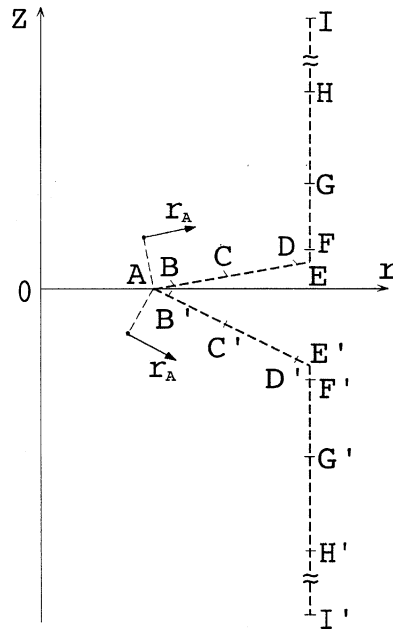
Fig. 4. Prospective boundary for notched bar and boundary division.

$$F_{\theta,\lambda_3}^{\text{III}} \propto r_A^{\lambda_3-1}(\lambda_3=1) \qquad F_{\theta,\lambda_4}^{\text{III}} \propto r_A^{\lambda_4-1}$$

(a)Symmetric (b)Skew-symmetric
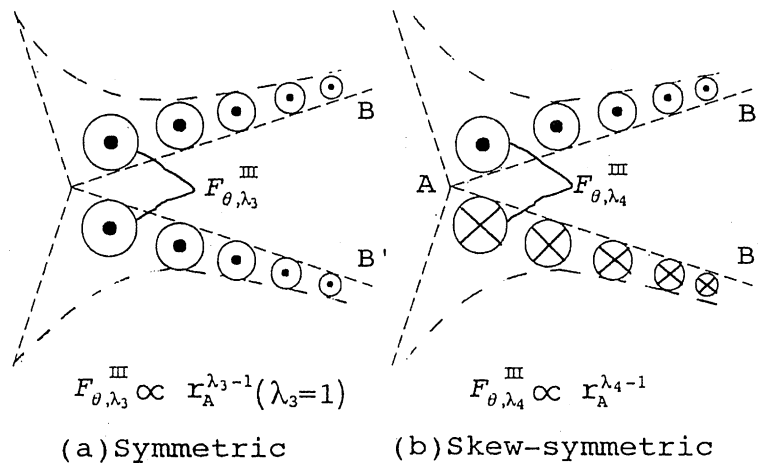
Fig. 5. Two types of body forces distributed along the angular corner.

functions, $r_A^{\lambda_3-1}$ and $r_A^{\lambda_4-1}$. Here, r_A is a distance measured from the notch A, and the eigenvalues λ_3 and λ_4 are given as the roots of eigenequations. Actually, we can put $\lambda_3 = 1$ for notch problem.

$$F_\theta(r_A) = F_\theta^{\text{III},\lambda_3}(r_A) + F_\theta^{\text{III},\lambda_4}(r_A) = W_\theta^{\text{III},\lambda_3}(r_A)r_A^{\lambda_3-1} + W_\theta^{\text{III},\lambda_4}(r_A)r_A^{\lambda_4-1}$$

$$W_\theta^{\text{III},\lambda_3}(r_A) = \sum_{n=1}^{M} a_n r_A^{n-1}, \quad W_\theta^{\text{III},\lambda_4}(r_A) = \sum_{n=1}^{M} b_n r_A^{n-1} \tag{13}$$

Except around the notch tip the body forces are simply approximated by using power series without using two types of distributions. On the numerical solution as shown in Eq. (13), the singular integral Eq. (12) is reduced to algebraic equations for the determination of the unknown coefficients, a_n, b_n. These coefficients are determined from the boundary conditions at suitably chosen collocation points. The generalized stress intensity factor K_{III,λ_4} for V-Shaped notch can be obtained from the value of $W_\theta^{III}(0)$ at the corner tip.

In tension of notched bar, body forces are distributed in the r- and z-directions; in bending, body forces are distributed in the r-, θ-, and z-directions [17]. In bending, generalized stress intensity factors are proportional as $K_{I,\lambda_1} \propto \cos\theta$, $K_{II,\lambda_2} \propto \cos\theta$, $K_{III,\lambda_4} \propto \sin\theta$; therefore, in the following sections, K_{I,λ_1}, K_{II,λ_2} at $\theta = 0$, and K_{III,λ_4} at $\theta = \pi/2$ will be discussed.

5. Results and discussion

In the following discussion, dimensionless stress intensity factors are defined in Eq. (14).
(1) *Torsion*

$$F_{III,\lambda_4} = K_{III,\lambda_4}/\tau^\infty\sqrt{\pi}t^{1-\lambda_4}, \quad \tau^\infty = \frac{16T}{\pi d^3}, \quad T = \text{torsional moment}$$

(2) *Tension*

$$F_{I,\lambda_1} = K_{I,\lambda_1}/\sigma^\infty\sqrt{\pi}t^{1-\lambda_1}, \quad F_{II,\lambda_2} = K_{II,\lambda_2}/\sigma^\infty\sqrt{\pi}t^{1-\lambda_2}, \quad \sigma^\infty = \frac{4P}{\pi d^2}, \quad P = \text{axial force}$$

(3) *Bending*

$$F_{I,\lambda_1} = K_{I,\lambda_1}/\sigma^\infty\sqrt{\pi}t^{1-\lambda_1}, \quad F_{II,\lambda_2} = K_{II,\lambda_2}/\sigma^\infty\sqrt{\pi}t^{1-\lambda_2}, \quad F_{III,\lambda_4} = K_{III,\lambda_4}/\sigma^\infty\sqrt{\pi}t^{1-\lambda_4},$$

$$\sigma^\infty = \frac{32M}{\pi d^3}, \quad M = \text{bending moment} \tag{14}$$
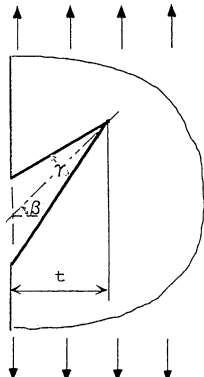
5.1. V-Shaped notched semi-infinite plate

First of all, limiting solutions in Fig. 1 will be considered when $2t/D \to 0$. In the previous study, a V-shaped notched semi-infinite plate under tension was analyzed [18]. The results are shown in Table 1 again as a limiting solution for tension and bending. However, since there is no solution for torsion problem, V-shaped notched semi-infinite plate under shear as shown in Fig. 6 is analyzed. Here, two different methods were used and their accuracy is compared. Here, method 1 uses the imaginary boundary of Fig. 7(a) for the body force distribution; method 2 uses the imaginary boundary of Fig. 7(b). Table 2 shows the convergence of the results of methods 1 and 2 with varying the number of polynomial M. Both results have good convergence and coincide with each other by the fifth digit. The difference between the results of methods 1 and 2 is within 0.01%. Table 3 shows the final results obtained using method 1.

5.2. Convergence of the results in Fig. 1

Generalized stress intensity factors F_{III,λ_4} under torsion are shown in Table 4(A) with varying the number of polynomial M. The results have good convergence to the fifth digit when $M = 8$–11. Generalized stress

Table 1
Results of a V-notch in a semi-infinite plate under tension

γ	F_{I,λ_1}				F_{II,λ_2}			
	$\beta = 0°$	$\beta = 15°$	$\beta = 30°$	$\beta = 45°$	$\beta = 0°$	$\beta = 15°$	$\beta = 30°$	$\beta = 45°$
15°	1.129	1.093	0.992	0.837	0.000	0.193	0.356	0.462
30°	1.148	1.107	1.000	0.834	0.000	0.218	0.397	0.505
45°	1.181	1.139	1.020	0.835	0.000	0.258	0.464	0.573
60°	1.225	1.176	1.040	0.824	0.000	0.326	0.577	0.684
90°	1.336	1.266	1.065		0.000	0.946	1.576	
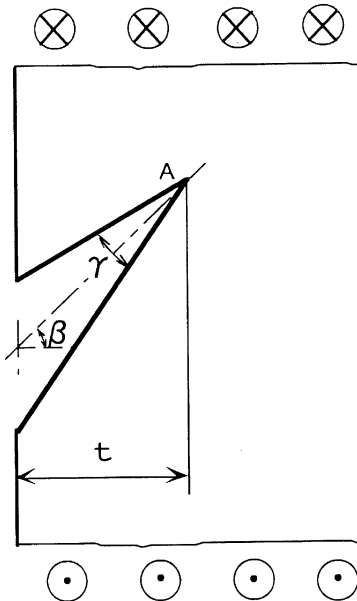
Fig. 6. Notched semi-infinite plate under shear: limiting solution when $2t/D \rightarrow 0$ in Fig. 1.

intensity factors F_{I,λ_1}, F_{II,λ_2} and F_{III,λ_4} under bending are shown in Table 4(B). The results have good convergence. The average value coincide with each other to the fourth digit when $M = 8$–10.

5.3. Results of a circumferential crack in a round bar

In this section the results of a crack, $\gamma = 0°$ under torsion and bending are obtained from the calculation for the small γ. Table 5 indicates results under torsion when $\gamma = 10°$, 15°, 30° and $\beta = 0$. In Table 5(A), F_{III,λ_4} values are normalized by the results when $\lambda = 2t/D \rightarrow 0$. As shown in Table 4(A), the values of

(a) Method 1   (b) Method 2
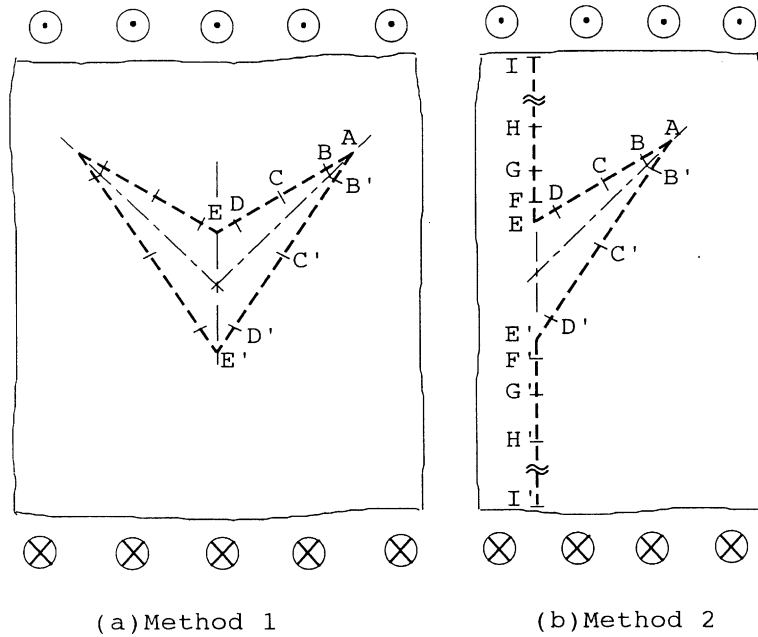
Fig. 7. Prospective boundaries for V-notch in methods 1 and 2.

Table 2
Convergence of $F_{\mathrm{III},\lambda_4}$ in Figs. 6 and 7

M	$\beta = 0°$				$\beta = 30°$
	$\gamma = 15°$	$\gamma = 30°$	$\gamma = 60°$	$\gamma = 90°$	$\gamma = 45°$
Method 1					
4	1.02445	1.05397	1.13513	1.26901	1.02190
5	1.02454	1.05410	1.13525	1.26916	1.02251
6	1.02454	1.05410	1.13526	1.26917	1.02250
7	1.02456	1.05412	1.13527	1.26920	1.02254
Method 2					
6	1.02336	1.05315	1.13505	1.26913	1.02199
7	1.02402	1.05339	1.13517	1.26916	1.02245
8	1.02431	1.05377	1.13549	1.26916	1.02252
9	1.02430	1.05418	1.13521	1.26911	1.02259
Ref. [2]	1.025	1.054	1.135	1.270	

$(1 - \lambda)^3 F_{\mathrm{III},\lambda_4}/F_{\mathrm{III},\lambda_4}|_{\lambda \to 0}$ are almost independent of γ. The extrapolated values $\gamma = 0°$ (15–10) are also obtained from the results of $\gamma = 15°$ and $\gamma = 10°$. Since the results of $\gamma = 0°$ (15–10) coincides with the values of $\gamma = 0°$ (30–15) to the third digit, F_{III}, values when $\gamma \to 0$ in Table 5(B) seems to have three digit accuracy. Table 5(B) also shows the values of Benthem–Koiter's formula [1] given by Eq. (15), and the ratio to the present results. As shown in Table 5(B) and Fig. 8, Benthem–Koiter's formula are found to have about 1% error.

Table 3
Results of a V-notch in a semi-infinite plate under shear

	γ	F_{III,λ_4}, method 1			
		$\beta = 0°$	$\beta = 15°$	$\beta = 30°$	$\beta = 45°$
	10°	1.0159	1.0042	0.9693	0.9103
	15°	1.0245	1.0124	0.9756	0.9139
	30°	1.0541	1.0399	0.9970	0.9242
	45°	1.0902	1.0734	1.0225	0.9353
	60°	1.1353	1.1150	1.0533	0.9453
	90°	1.2692	1.2372	1.1369	

Table 4
Convergence of F_{I,λ_1}, F_{II,λ_2}, F_{III,λ_4} in Fig. 1: (A) F_{III,λ_4} for torison, (B) F_{I,λ_1}, F_{II,λ_2}, F_{III,λ_4} for bending
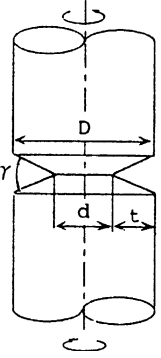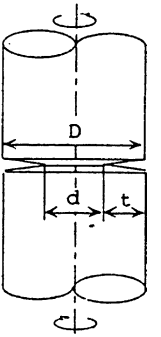
M	$\gamma = 30°$, $\lambda_4 = 0.5454545$, $\lambda = 2t/D = 0.2$				
	$\beta = 0°$	$\beta = 15°$	$\beta = 30°$	$\beta = 45°$	
A: F_{III,λ_4} for torison					
8	1.36668	1.35002	1.30046	1.21905	
9	1.36676	1.35011	1.30050	1.21886	
10	1.36682	1.35018	1.30055	1.21881	
11	1.36683	1.35018	1.30052	1.21868	
	$\gamma = 60°$, $\lambda_4 = 0.6$, $\lambda = 2t/D = 0.5$				
8	3.74436	3.70312	3.58159	3.38597	
9	3.74434	3.70312	3.58162	3.38597	
10	3.74433	3.70312	3.58167	3.38604	
11	3.74432	3.70311	3.58166	3.38598	

M_1	F_{I,λ_1} ($\lambda_1 = 0.5050097$)			F_{II,λ_2} ($\lambda_2 = 0.6597016$)			F_{III,λ_4}
	From $W_n^{\text{I}}(0)$	From $W_t^{\text{I}}(0)$	Average	From $W_n^{\text{II}}(0)$	From $W_t^{\text{II}}(0)$	Average	From $W_0^{\text{III}}(0)$
B: F_{I,λ_1}, F_{II,λ_2}, F_{III,λ_4} for bending							
6	3.0912	3.0913	3.0913	0.5894	0.5900	0.5897	0.6521
7	3.0969	3.0969	3.0969	0.5722	0.5726	0.5724	0.6399
8	3.0986	3.0985	3.0985	0.5672	0.5676	0.5674	0.6293
9	3.1003	3.1001	3.1002	0.5612	0.5615	0.5613	0.6183
10	3.0999	3.0995	3.0997	0.5612	0.5614	0.5613	0.6184

$$F_{\text{III},B}\xi = \frac{3}{8}\xi^{-5/2}\left(1 + \frac{1}{2}\xi + \frac{3}{8}\xi^2 + \frac{5}{16}\xi^3 + \frac{35}{128}\xi^4 + 0.208\xi^5\right), \quad \xi = d/D \tag{15}$$

By applying the least squares method to the ratio $F_{\text{III},(15-10)}/F_{\text{III},B}$ in Fig. 8, more accurate formula is proposed. Eq. (16) with Eq. (15) gives accurate values with less than 0.2% estimated errors.

Table 5
Results of a circumferential crack in a round bar under torsion: (A) $(1 - \lambda)^3 F_{III,\lambda_4}/F_{III,\lambda_4}|_{\lambda \to 0}$, $\lambda = 2t/D$, (B) F_{III} and Benthem–Koiter's value $F_{III,B}$

	$\lambda = 2t/D$	$\gamma = 10°$	$\gamma = 15°$	$\gamma = 30°$	$\gamma = 0°$ (15–10)	$\gamma = 0°$ (30–15)
	A: $(1 - \lambda)^3 F_{III,\lambda_4}/F_{III,\lambda_4}|_{\lambda \to 0}$					
	0.01	0.9798	0.9797	0.9789	0.9800	0.9805
	0.02	0.9574	0.9578	0.9568	0.9566	0.9588
	0.05	0.8961	0.8964	0.8954	0.8955	0.8974
	0.1	0.8064	0.8067	0.8062	0.8058	0.8072
	0.2	0.6617	0.6625	0.6640	0.6601	0.6610
	0.3	0.5490	0.5504	0.5540	0.5462	0.5468
	0.4	0.4576	0.4596	0.4635	0.4536	0.4557
	0.5	0.3812	0.3837	0.3912	0.3762	0.3762
	0.6	0.3148	0.3177	0.3267	0.3090	0.3087
	0.7	0.2545	0.2576	0.2676	0.2483	0.2476
	0.8	0.1960	0.1992	0.2095	0.1896	0.1889
	0.9	0.1322	0.1352	0.1449	0.1262	0.1255

	$\lambda = 2t/D$	$F_{III,(15-10)}$, $\gamma \to 0°$	$F_{III,(30-15)}$, $\gamma \to 0°$	$F_{III,B}$	$F_{III,(15-10)}/F_{III,B}$	$F_{III,(30-15)}/F_{III,B}$
	B: F_{III} and Benthem–Koiter's value $F_{III,B}$					
	0.01	1.0100	1.0105	1.0099	1.0001	1.0006
	0.02	1.0164	1.0187	1.0194	0.9971	0.9993
	0.05	1.0445	1.0467	1.0509	0.9949	0.9960
	0.1	1.1053	1.1072	1.1145	0.9917	0.9934
	0.2	1.2893	1.2910	1.2972	0.9939	0.9952
	0.3	1.5924	1.5942	1.5930	0.9996	1.0008
	0.4	2.1000	2.1097	2.0899	1.0048	1.0095
	0.5	3.0096	3.0096	2.9834	1.0088	1.0088
	0.6	4.8281	4.8234	4.7770	1.0107	1.0097
	0.7	9.1693	9.1704	9.0900	1.0087	1.0088
	0.8	23.700	23.613	23.437	1.0112	1.0075
	0.9	126.20	125.50	125.00	1.0096	1.0040

$$F_{III}/F_{III,B} = 1.0009 - 0.19064\lambda + 1.2326\lambda^2 - 2.7484\lambda^3 + 2.7081\lambda^4 - 1.0024\lambda^5, \quad \lambda = 2t/D \tag{16}$$

Similarly, for bending, Table 6 and Fig. 9 indicate the results of a crack in comparison with Benthem–Koiter's values.

$$F_{I,B} = \frac{3}{8} \xi^{-5/2} \left\{ 1 + \frac{1}{2}\xi + \frac{3}{8}\xi^2 + \frac{5}{16}\xi^3 + \frac{35}{128}\xi^4 + 0.531\xi^5 \right\}, \quad \xi = d/D \tag{17}$$

In bending, Benthem–Koiter's formula are found to have about 3% error. By applying the least squares method, more accurate formula is proposed. Eq. (18) with Eq. (17) gives accurate values with less than 0.3% estimated errors.

$$F_I/F_{I,B} = 1.0002 - 0.5226\lambda + 3.1062\lambda^2 - 6.7504\lambda^3 + 6.5459\lambda^4 - 2.3794\lambda^5, \quad \lambda = 2t/D \tag{18}$$

5.4. Results of 60° V-notched bar as limiting solutions in fatigue test specimens

60° V-notched bar with a notch root radius ρ has been often used as fatigue test specimens. Table 7 shows $K_t/K_t|_{\lambda = 2t/D \to 0}$ when $2\rho/D = 0.03, 0.05$ under tension in comparison with the present results. Since all results
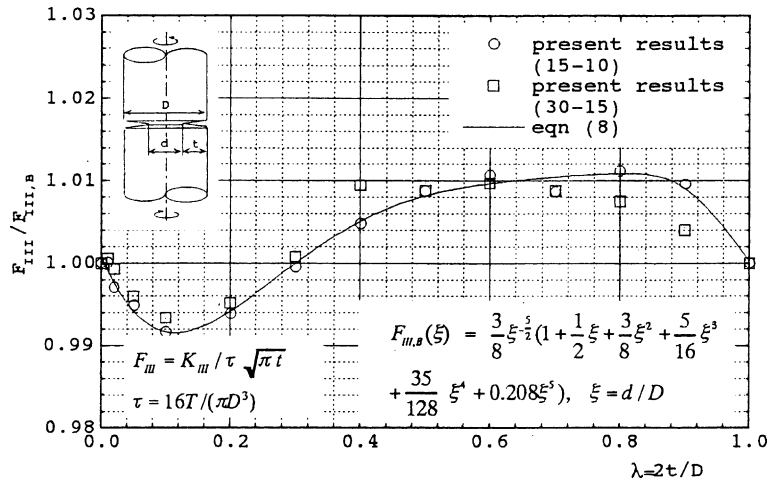
Fig. 8. $F_{III}/F_{III,B}$ vs. $\lambda = 2t/D$ under torsion.

Table 6
Results of a circumferential crack in a round bar under bending

	$\lambda = 2t/D$	$(1-\lambda)^3 F_{I,\lambda_1}/F_{I,\lambda_1}\|_{\lambda \to 0}$		$F_I, \gamma = 0°$	$F_{I,B}$	$F_I/F_{I,B}$ ( ): Eq. (9)
		$\gamma = 15°$	$\gamma = 30°$			
	0.05	0.869	0.869	1.137	1.158	0.982 (0.981)
	0.1	0.765	0.762	1.177	1.211	0.972 (0.973)
	0.2	0.608	0.608	1.332	1.363	0.978 (0.976)
	0.3	0.495	0.495	1.618	1.643	0.985 (0.988)
	0.4	0.408	0.407	2.118	2.117	1.001 (0.999)
	0.5	0.337	0.336	3.024	3.000	1.008 (1.006)
	0.6	0.276	0.276	4.836	4.800	1.008 (1.010)
	0.7	0.222	0.222	9.221	9.100	1.013 (1.013)
	0.8	0.170	0.170	23.83	23.45	1.016 (1.016)
	0.9	0.113	0.113	126.7	125.0	1.014 (1.014)

coincide with each other with less than 1% errors when $\lambda = 2t/D \leqslant 0.7$, we can estimate accurate stress concentration factors even for very small radius of ρ. Table 8 shows the results under bending. In bending all results coincide with each other within about 1% error when $\lambda = 2t/D \leqslant 0.5$.

5.5. General results in Fig. 1

Figs. 10 and 11 show the relation between stress intensity factors and $2t/D$. For example, Fig. 10(a) shows the relation between $(1-\lambda)^3 F_{III,\lambda_4}/F_{III,\lambda_4}\|_{\lambda \to 0}$ and $2t/D$ with varying opening angle γ in the range 15–90° for torsion problem. From Fig. 10(a)–(c), it is seen that the variations of normalized stress intensity factors $(1-\lambda)^3 F_{III,\lambda_4}/F_{III,\lambda_4}\|_{\lambda \to 0}$ are small if $2t/D$ is constant, almost independent of β and γ. From
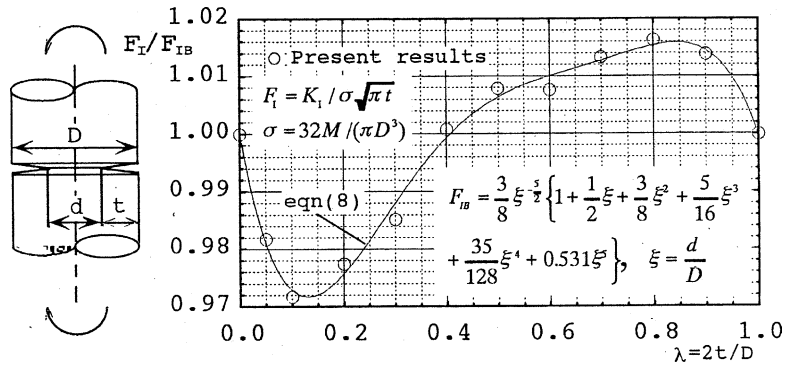
Fig. 9. $F_I/F_{I,B}$ vs. $\lambda = 2t/D$ under bending.

Table 7
$K_t/K_{tS}(K_{tS} = K_t|_{\lambda \to 0})$ of a notched bar with a root radius ρ under tension
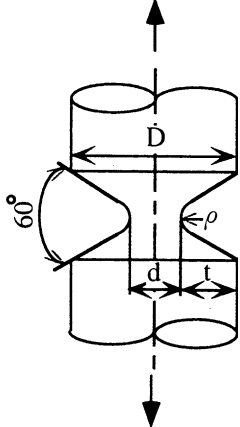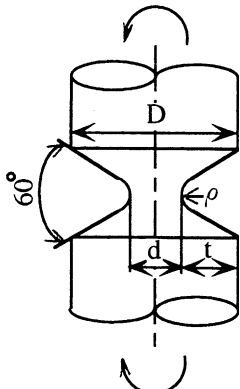
$\lambda = 2t/D$	$2\rho/D$		
	$\to 0$ (Table 10(D))	0.02 [2,17]	0.03 [2,17]
0.02	0.970	0.964	0.968
0.05	0.928	0.923	0.921
0.1	0.854	0.847	0.849
0.2	0.724	0.716	0.717
0.3	0.613	0.608	0.608
0.4	0.519	0.517	0.516
0.5	0.437	0.436	0.435
0.6	0.363	0.363	0.363
0.7	0.294	0.296	0.296
0.8	0.226	0.230	0.232
0.9	0.152	0.160	0.165

Table 8
$K_t/K_{tS}(K_{tS} = K_t|_{\lambda \to 0})$ of a notched bar with a root radius ρ under bending

$\lambda = 2t/D$	$2\rho/D$		
	$\to 0$ (Table 11(D))	0.03 [2,17]	0.05 [2,17]
0.02	0.937	0.937	0.936
0.05	0.867	0.860	0.858
0.1	0.762	0.751	0.753
0.2	0.605	0.597	0.597
0.3	0.492	0.487	0.488
0.4	0.405	0.403	0.405
0.5	0.335	0.337	0.339
0.6	0.276	0.281	0.284
0.7	0.222	0.230	0.235
0.8	0.171	0.182	0.189
0.9	0.115	0.132	0.143
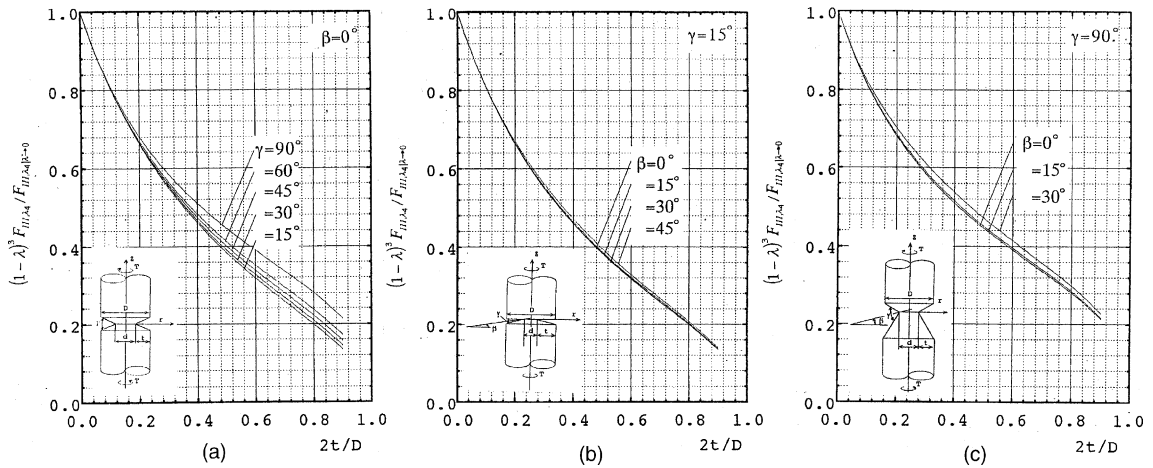
Fig. 10. Results of torsion: (a) $(1-\lambda)^3 F_{III,\lambda_4}/F_{III,\lambda_4}|_{\lambda\to0}$ vs. $2t/D$ for $\beta = 0°$, (b) $(1-\lambda)^3 F_{III,\lambda_4}/F_{III,\lambda_4}|_{\lambda\to0}$ vs. $2t/D$ for $\gamma = 15°$, (c) $(1-\lambda)^3 F_{III,\lambda_4}/F_{III,\lambda_4}|_{\lambda\to0}$ vs. $2t/D$ for $\gamma = 90°$.
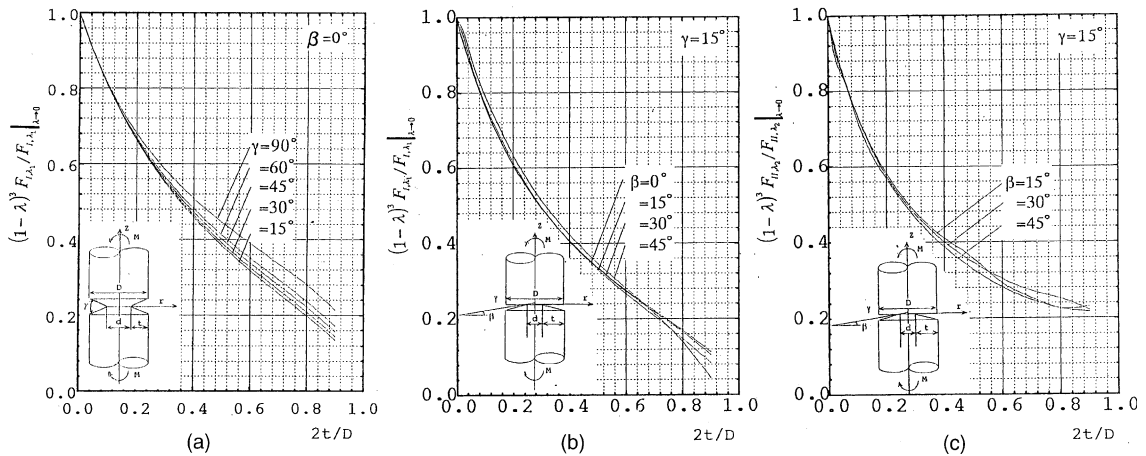
Fig. 11. Results of bending: (a) $(1-\lambda)^3 F_{I,\lambda_1}/F_{I,\lambda_1}|_{\lambda\to0}$ vs. $2t/D$ for $\beta = 0°$, (b) $(1-\lambda)^3 F_{I,\lambda_1}/F_{I,\lambda_1}|_{\lambda\to0}$ vs. $2t/D$ for $\gamma = 15°$, (c) $(1-\lambda)^3 F_{II,\lambda_2}/F_{II,\lambda_2}|_{\lambda\to0}$ vs. $2t/D$ for $\gamma = 15°$.

Fig. 11(a)–(c), it is also seen that the variations of $(1 - \lambda)^3 F_{I,\lambda_1}/F_{I,\lambda_1}|_{\lambda\to0}$ and $(1 - \lambda)^3 F_{II,\lambda_2}/F_{II,\lambda_2}|_{\lambda\to0}$ are small also for bending.

Generalized stress intensity factors at the notch tip for each problems are systematically calculated for various shapes of V-shaped notches. In Tables 9–11, the values of $(1 - \lambda)^3 F_{III,\lambda_4}/F_{III,\lambda_4}|_{\lambda\to0}$ and for torsion, the values of $(1 - \lambda)^3 F_{I,\lambda_1}/F_{I,\lambda_1}|_{\lambda\to0}$ and $(1 - \lambda)^3 F_{II,\lambda_2}/F_{II,\lambda_2}|_{\lambda\to0}$ for tension and bending are shown. As shown in Tables 9–11, the variations of those normalized values are small for the wide range of γ and β if $2t/D$ is constant. For bending F_{III,λ_4} values are shown without normalizing because in this case normalizing is

Table 9
Results of V-notched bar under torsion: (A) $\gamma = 15°$, (B) $\gamma = 30°$, (C) $\gamma = 45°$, (D) $\gamma = 60°$, (E) $\gamma = 90°$

$\lambda = 2t/D$	$(1 - \lambda)^3 F_{III,\lambda_4}/F_{III,\lambda_4\|\lambda\to 0}$			
	$\beta = 0°$	$\beta = 15°$	$\beta = 30°$	$\beta = 45°$
A: $\gamma = 15°$, $\lambda_4 = 0.521739$				
$\to 0$	1.000	1.000	1.000	1.000
0.01	0.980	0.980	0.979	0.978
0.02	0.958	0.958	0.957	0.956
0.05	0.896	0.896	0.896	0.896
0.1	0.807	0.807	0.807	0.808
0.2	0.663	0.663	0.665	0.669
0.3	0.550	0.551	0.554	0.561
0.4	0.460	0.461	0.464	0.472
0.5	0.384	0.385	0.388	0.396
0.6	0.318	0.319	0.322	0.329
0.7	0.258	0.259	0.262	0.268
0.8	0.199	0.200	0.202	0.207
0.9	0.135	0.136	0.137	0.140
B: $\gamma = 30°$, $\lambda_4 = 0.5454545$				
$\to 0$	1.000	1.000	1.000	1.000
0.01	0.979	0.979	0.979	0.979
0.02	0.957	0.957	0.957	0.957
0.05	0.895	0.895	0.896	0.897
0.1	0.806	0.806	0.808	0.811
0.2	0.664	0.665	0.668	0.675
0.3	0.554	0.555	0.560	0.570
0.4	0.465	0.467	0.472	0.483
0.5	0.391	0.393	0.398	0.409
0.6	0.327	0.328	0.333	0.343
0.7	0.268	0.269	0.273	0.281
0.8	0.209	0.210	0.214	0.221
0.9	0.145	0.146	0.148	0.153
C: $\gamma = 45°$, $\lambda_4 = 0.571428$				
$\to 0$	1.000	1.000	1.000	1.000
0.01	0.979	0.979	0.978	0.978
0.02	0.956	0.956	0.956	0.957
0.05	0.895	0.895	0.895	0.897
0.1	0.807	0.807	0.808	0.814
0.2	0.666	0.668	0.672	0.683
0.3	0.559	0.561	0.567	0.582
0.4	0.473	0.475	0.482	0.498
0.5	0.401	0.403	0.410	0.425
0.6	0.338	0.340	0.346	0.360
0.7	0.280	0.281	0.287	0.299
0.8	0.222	0.233	0.228	0.238
0.9	0.157	0.158	0.161	0.168
D: $\gamma = 60°$, $\lambda_4 = 0.6$				
$\to 0$	1.000	1.000	1.000	1.000
0.01	0.978	0.978	0.978	0.978
0.02	0.956	0.956	0.956	0.957
0.05	0.895	0.895	0.896	0.899
0.1	0.807	0.808	0.811	0.819

Table 9 (*continued*)

$\lambda = 2t/D$	$(1-\lambda)^3 F_{\mathrm{III},\lambda_4}/F_{\mathrm{III},\lambda_4}|_{\lambda \to 0}$			
	$\beta = 0°$	$\beta = 15°$	$\beta = 30°$	$\beta = 45°$
0.2	0.670	0.671	0.678	0.696
0.3	0.565	0.568	0.577	0.600
0.4	0.482	0.485	0.495	0.519
0.5	0.412	0.415	0.425	0.448
0.6	0.351	0.354	0.363	0.383
0.7	0.295	0.297	0.305	0.322
0.8	0.237	0.239	0.246	0.260
0.9	0.172	0.173	0.178	0.188
E: γ = 90°, $\lambda_4 = 0.6666667$				
→ 0	1.000	1.000	1.000	
0.01	0.977	0.977	0.977	
0.02	0.955	0.955	0.956	
0.05	0.895	0.895	0.898	
0.1	0.810	0.812	0.820	
0.2	0.681	0.685	0.702	
0.3	0.585	0.590	0.611	
0.4	0.509	0.515	0.537	
0.5	0.446	0.451	0.472	
0.6	0.390	0.395	0.414	
0.7	0.336	0.341	0.357	
0.8	0.281	0.258	0.299	
0.9	0.214	0.217	0.228	

not effective. For other cases we can estimate any dimensions of notches easily from those normalized results.

6. Conclusions

In this study, generalized stress intensity factors K_{I,λ_1}, $K_{\mathrm{II},\lambda_2}$, and $K_{\mathrm{III},\lambda_4}$ are systematically calculated for a V-shaped notched round test specimens under torsion, tension, and bending using the singular integral equation of the body force method.

(1) In the numerical solution of the singular integral equation of the body force method, the unknown body force densities are approximated by piecewise smooth functions using power series and two types of fundamental density functions. The results shows that the present method gives rapidly converging numerical results.

(2) In Tables 9–11, the values of $(1-\lambda)^3 F_{\mathrm{III},\lambda_4}/F_{\mathrm{III},\lambda_4}|_{\lambda \to 0}$ for torsion, the values of $(1-\lambda)^3 F_{\mathrm{I},\lambda_1}/F_{\mathrm{I},\lambda_1}|_{\lambda \to 0}$ and $(1-\lambda)^3 F_{\mathrm{II},\lambda_2}/F_{\mathrm{II},\lambda_2}|_{\lambda \to 0}$ for tension and bending are shown with varying γ, β, and $2t/D$ systematically. It is found that if $2t/D$ is constant the variations of those normalized values are small for the wide range of γ and β. We can estimate any dimensions of notches from those normalized results.

(3) Benthem–Koiter's formula are found to have 1–3% error. More accurate formulas are proposed with less than 0.3% estimated errors.

(4) 60° V-notched bar with a notch root radius ρ has been often used as fatigue test specimens. For small ρ the results of normalized stress concentration factors $K_t/K_t|_{\lambda=2t/D \to 0}$ coincide with the present analysis with less than 1% errors. Therefore we can estimate accurate stress concentration factors even for very small radius of ρ.

Table 10
Results of V-notched bar under tension: (A) $\gamma = 15°$, (B) $\gamma = 30°$, (C) $\gamma = 45°$, (D) $\gamma = 60°$, (E) $\gamma = 90°$

$\lambda = 2t/D$	$(1-\lambda)^2 F_{I,\lambda_1}/F_{I,\lambda_1}|_{\lambda \to 0}$				$(1-\lambda)^2 F_{II,\lambda_2}/F_{II,\lambda_2}|_{\lambda \to 0}$			
	$\beta = 0°$	$\beta = 15°$	$\beta = 30°$	$\beta = 45°$	$\beta = 0°$	$\beta = 15°$	$\beta = 30°$	$\beta = 45°$
A: $\gamma = 15°$, $\lambda_1 = 0.5001793$, $\lambda_2 = 0.5452545$								
$\to 0$	1.000	1.000	1.000	1.000	0.000	1.000	1.000	1.000
0.01	0.987	0.990	0.995	1.002	0.000	0.970	0.966	0.967
0.02	0.973	0.975	0.982	0.989	0.000	0.955	0.950	0.952
0.05	0.930	0.933	0.939	0.948	0.000	0.907	0.905	0.904
0.1	0.857	0.858	0.862	0.867	0.000	0.844	0.840	0.840
0.2	0.725	0.726	0.727	0.727	0.000	0.720	0.719	0.723
0.3	0.613	0.613	0.612	0.605	0.000	0.622	0.624	0.633
0.4	0.518	0.518	0.514	0.504	0.000	0.543	0.543	0.555
0.5	0.436	0.435	0.429	0.419	0.000	0.468	0.471	0.483
0.6	0.362	0.360	0.354	0.346	0.000	0.398	0.400	0.413
0.7	0.293	0.291	0.286	0.279	0.000	0.328	0.331	0.343
0.8	0.225	0.223	0.219	0.214	0.000	0.256	0.260	0.271
0.9	0.150	0.149	0.146	0.143	0.000	0.176	0.180	0.189
B: $\gamma = 30°$, $\lambda_1 = 0.5014530$, $\lambda_2 = 0.5981918$								
$\to 0$	1.000	1.000	1.000	1.000	0.000	1.000	1.000	1.000
0.01	0.984	0.987	0.992	1.000	0.000	0.985	0.980	0.972
0.02	0.972	0.976	0.980	0.988	0.000	0.969	0.965	0.958
0.05	0.930	0.934	0.938	0.947	0.000	0.919	0.918	0.911
0.1	0.856	0.860	0.861	0.868	0.000	0.847	0.845	0.842
0.2	0.725	0.728	0.729	0.733	0.000	0.719	0.719	0.719
0.3	0.614	0.617	0.615	0.617	0.000	0.614	0.617	0.621
0.4	0.519	0.519	0.518	0.520	0.000	0.528	0.531	0.540
0.5	0.437	0.436	0.435	0.436	0.000	0.451	0.454	0.467
0.6	0.363	0.362	0.361	0.363	0.000	0.378	0.384	0.402
0.7	0.293	0.293	0.293	0.294	0.000	0.310	0.317	0.339
0.8	0.225	0.225	0.225	0.226	0.000	0.242	0.252	0.274
0.9	0.151	0.151	0.151	0.151	0.000	0.170	0.181	0.199
C: $\gamma = 45°$, $\lambda_1 = 0.5050097$, $\lambda_2 = 0.6597016$								
$\to 0$	1.000	1.000	1.000	1.000	0.000	1.000	1.000	1.000
0.01	0.982	0.984	0.985	1.001	0.000	0.984	0.978	0.980
0.02	0.971	0.972	0.975	0.998	0.000	0.968	0.965	0.972
0.05	0.929	0.930	0.933	0.939	0.000	0.920	0.918	0.914
0.1	0.855	0.856	0.858	0.863	0.000	0.848	0.845	0.841
0.2	0.725	0.725	0.727	0.735	0.000	0.717	0.714	0.715
0.3	0.614	0.614	0.616	0.627	0.000	0.610	0.608	0.613
0.4	0.519	0.520	0.522	0.535	0.000	0.516	0.518	0.530
0.5	0.437	0.437	0.440	0.455	0.000	0.434	0.438	0.461
0.6	0.363	0.364	0.368	0.382	0.000	0.360	0.368	0.400
0.7	0.294	0.295	0.299	0.312	0.000	0.292	0.306	0.343
0.8	0.225	0.227	0.231	0.241	0.000	0.230	0.248	0.285
0.9	0.151	0.152	0.155	0.162	0.000	0.168	0.185	0.216
D: $\gamma = 60°$, $\lambda_1 = 0.5122214$, $\lambda_2 = 0.7309007$								
$\to 0$	1.000	1.000	1.000	1.000	0.000	1.000	1.000	1.000
0.01	0.983	0.983	0.984	0.990	0.000	0.992	0.983	0.982
0.02	0.970	0.972	0.971	0.978	0.000	0.972	0.967	0.966
0.05	0.928	0.929	0.931	0.936	0.000	0.930	0.917	0.916
0.1	0.854	0.855	0.857	0.864	0.000	0.847	0.842	0.842

(*continued on next page*)

Table 10 (*continued*)

$\lambda = 2t/D$	$(1-\lambda)^2 F_{\mathrm{I},\lambda_1}/F_{\mathrm{I},\lambda_1}\vert_{\lambda\to 0}$				$(1-\lambda)^2 F_{\mathrm{II},\lambda_2}/F_{\mathrm{II},\lambda_2}\vert_{\lambda\to 0}$			
	$\beta = 0°$	$\beta = 15°$	$\beta = 30°$	$\beta = 45°$	$\beta = 0°$	$\beta = 15°$	$\beta = 30°$	$\beta = 45°$
0.2	0.724	0.729	0.731	0.745	0.000	0.707	0.703	0.715
0.3	0.613	0.608	0.613	0.646	0.000	0.600	0.597	0.615
0.4	0.519	0.516	0.523	0.562	0.000	0.502	0.505	0.536
0.5	0.437	0.436	0.446	0.485	0.000	0.417	0.426	0.470
0.6	0.363	0.364	0.375	0.411	0.000	0.342	0.359	0.414
0.7	0.294	0.296	0.308	0.337	0.000	0.278	0.303	0.361
0.8	0.226	0.229	0.240	0.262	0.000	0.224	0.252	0.309
0.9	0.152	0.155	0.162	0.178	0.000	0.172	0.198	0.247
E: $\gamma = 90°$, $\lambda_1 = 0.5444837$, $\lambda_2 = 0.9085292$								
$\to 0$	1.000	1.000	1.000		0.000	1.000	1.000	
0.01	0.985	0.985	0.983		0.000	0.984	0.982	
0.02	0.971	0.972	0.971		0.000	0.970	0.967	
0.05	0.927	0.928	0.928		0.000	0.921	0.919	
0.1	0.852	0.854	0.856		0.000	0.843	0.840	
0.2	0.722	0.724	0.736		0.000	0.701	0.703	
0.3	0.612	0.616	0.640		0.000	0.578	0.591	
0.4	0.518	0.525	0.558		0.000	0.472	0.503	
0.5	0.434	0.446	0.485		0.000	0.385	0.434	
0.6	0.365	0.375	0.414		0.000	0.320	0.382	
0.7	0.298	0.309	0.345		0.000	0.276	0.341	
0.8	0.233	0.242	0.273		0.000	0.248	0.310	
0.9	0.161	0.168	0.189		0.000	0.229	0.282	

Table 11

Results of V-notched bar under bending: (A) $\gamma = 15°$, (B) $\gamma = 30°$, (C) $\gamma = 45°$, (D) $\gamma = 60°$, (E) $\gamma = 90°$

$\lambda = 2t/D$	$\lambda_1 = 0.5001793$, $\lambda_2 = 0.5452545$, $v = 0.3$								$\lambda_4 = 0.521739$			
	$\beta = 0°$	$\beta = 15°$	$\beta = 30°$	$\beta = 45°$	$\beta = 0°$	$\beta = 15°$	$\beta = 30°$	$\beta = 45°$	$\beta = 0°$	$\beta = 15°$	$\beta = 30°$	$\beta = 45°$
A: $\gamma = 15°$												
$\to 0$	1.000	1.000	1.000	1.000	0.000	1.000	1.000	1.000				
0.02	0.940	0.944	0.959	0.971	0.000	0.932	0.921	0.904	0.000	0.206	0.381	0.484
0.05	0.869	0.872	0.879	0.896	0.000	0.849	0.843	0.839	0.000	0.205	0.375	0.485
0.1	0.765	0.767	0.772	0.794	0.000	0.739	0.737	0.725	0.000	0.207	0.378	0.485
0.2	0.608	0.609	0.615	0.634	0.000	0.584	0.577	0.570	0.000	0.229	0.416	0.534
0.3	0.495	0.495	0.497	0.515	0.000	0.480	0.474	0.465	0.000	0.278	0.505	0.644
0.4	0.408	0.407	0.406	0.424	0.000	0.411	0.401	0.388	0.000	0.370	0.670	0.848
0.5	0.337	0.335	0.331	0.348	0.000	0.358	0.347	0.329	0.000	0.539	0.982	1.236
0.6	0.276	0.274	0.267	0.282	0.000	0.293	0.304	0.282	0.000	0.895	1.645	2.062
0.7	0.222	0.219	0.208	0.215	0.000	0.254	0.272	0.248	0.000	1.833	3.400	4.270
0.8	0.170	0.166	0.148	0.140	0.000	0.226	0.252	0.226	0.000	5.478	10.27	13.11
0.9	0.113	0.106	0.085	0.045	0.000	0.231	0.222	0.217	0.000	44.77	79.38	100.7
	$\lambda_1 = 0.5014530$, $\lambda_2 = 0.5981918$, $v = 0.3$								$\lambda_4 = 0.5454545$			
B: $\gamma = 30°$												
$\to 0$	1.000	1.000	1.000	1.000	0.000	1.000	1.000	1.000				
0.02	0.938	0.945	0.954	0.964	0.000	0.932	0.927	0.925	0.000	0.264	0.479	0.609
0.05	0.869	0.873	0.874	0.890	0.000	0.854	0.855	0.845	0.000	0.254	0.461	0.583
0.1	0.762	0.768	0.769	0.787	0.000	0.742	0.742	0.733	0.000	0.247	0.454	0.573
0.2	0.608	0.611	0.614	0.632	0.000	0.579	0.577	0.573	0.000	0.264	0.486	0.615
0.3	0.495	0.497	0.500	0.520	0.000	0.462	0.465	0.466	0.000	0.313	0.574	0.731

Table 11 (*continued*)

$\lambda = 2t/D$	$\lambda_1 = 0.5014530, \lambda_2 = 0.5981918, v = 0.3$								$\lambda_4 = 0.5454545$			
	$\beta = 0°$	$\beta = 15°$	$\beta = 30°$	$\beta = 45°$	$\beta = 0°$	$\beta = 15°$	$\beta = 30°$	$\beta = 45°$	$\beta = 0°$	$\beta = 15°$	$\beta = 30°$	$\beta = 45°$
0.4	0.407	0.410	0.412	0.431	0.000	0.378	0.386	0.391	0.000	0.393	0.743	0.958
0.5	0.336	0.339	0.339	0.357	0.000	0.304	0.327	0.334	0.000	0.538	1.076	1.399
0.6	0.276	0.279	0.277	0.289	0.000	0.241	0.282	0.291	0.000	0.827	1.798	2.361
0.7	0.222	0.225	0.219	0.219	0.000	0.181	0.249	0.262	0.000	1.518	3.734	4.996
0.8	0.170	0.174	0.159	0.139	0.000	0.117	0.231	0.248	0.000	3.770	11.72	15.82
0.9	0.113	0.120	0.087	0.035	0.000	0.020	0.242	0.257	0.000	12.33	100.4	130.5
	$\lambda_1 = 0.5050097, \lambda_2 = 0.6597016, v = 0.3$								$\lambda_4 = 0.5714285$			
C: $\gamma = 45°$												
$\to 0$	1.000	1.000	1.000	1.000	0.000	1.000	1.000	1.000				
0.02	0.937	0.939	0.942	0.951	0.000	0.932	0.928	0.929	0.000	0.360	0.645	0.797
0.05	0.868	0.869	0.871	0.882	0.000	0.854	0.851	0.846	0.000	0.334	0.599	0.737
0.1	0.763	0.764	0.767	0.781	0.000	0.739	0.735	0.733	0.000	0.319	0.573	0.706
0.2	0.607	0.608	0.613	0.634	0.000	0.569	0.569	0.574	0.000	0.330	0.594	0.740
0.3	0.493	0.496	0.502	0.526	0.000	0.444	0.454	0.470	0.000	0.371	0.684	0.873
0.4	0.406	0.410	0.417	0.441	0.000	0.348	0.371	0.398	0.000	0.452	0.870	1.144
0.5	0.336	0.340	0.348	0.365	0.000	0.272	0.309	0.346	0.000	0.616	1.242	1.688
0.6	0.276	0.281	0.288	0.294	0.000	0.209	0.260	0.310	0.000	0.987	2.063	2.901
0.7	0.222	0.228	0.232	0.221	0.000	0.156	0.223	0.286	0.000	1.994	4.239	6.263
0.8	0.170	0.176	0.175	0.140	0.000	0.105	0.197	0.276	0.000	6.706	13.25	20.17
0.9	0.114	0.119	0.106	0.038	0.000	0.055	0.195	0.291	0.000	59.94	112.5	168.6
	$\lambda_1 = 0.5122214, \lambda_2 = 0.7309007, v = 0.3$								$\lambda_4 = 0.600000$			
D: $\gamma = 60°$												
$\to 0$	1.000	1.000	1.000	1.000	0.000	1.000	1.000	1.000				
0.02	0.937	0.935	0.938	0.946	0.000	0.933	0.933	0.932	0.000	0.538	0.949	1.124
0.05	0.867	0.868	0.870	0.880	0.000	0.854	0.850	0.848	0.000	0.480	0.842	1.002
0.1	0.762	0.762	0.766	0.784	0.000	0.735	0.733	0.736	0.000	0.444	0.783	0.933
0.2	0.605	0.608	0.616	0.648	0.000	0.560	0.562	0.581	0.000	0.439	0.782	0.959
0.3	0.492	0.496	0.508	0.546	0.000	0.435	0.447	0.482	0.000	0.484	0.878	1.126
0.4	0.405	0.410	0.427	0.464	0.000	0.342	0.360	0.413	0.000	0.594	1.100	1.472
0.5	0.335	0.341	0.361	0.390	0.000	0.278	0.296	0.362	0.000	0.846	1.559	2.172
0.6	0.276	0.281	0.302	0.320	0.000	0.237	0.245	0.325	0.000	1.470	2.546	3.718
0.7	0.222	0.226	0.249	0.251	0.000	0.215	0.200	0.298	0.000	3.402	5.069	7.896
0.8	0.171	0.173	0.196	0.178	0.000	0.214	0.157	0.277	0.000	13.10	14.37	24.41
0.9	0.115	0.112	0.131	0.098	0.000	0.269	0.131	0.258	0.000	137.7	88.20	178.8
	$\lambda_1 = 0.5444837, \lambda_2 = 0.9085292, v = 0.3$								$\lambda_4 = 0.6666667$			
E: $\gamma = 90°$												
$\to 0$	1.000	1.000	1.000		0.000	1.000	1.000					
0.02	0.940	0.940	0.938		0.000	0.932	0.930		0.000	2.399	3.996	
0.05	0.866	0.867	0.869		0.000	0.843	0.844		0.000	1.918	3.202	
0.1	0.759	0.761	0.771		0.000	0.720	0.725		0.000	1.629	2.733	
0.2	0.601	0.607	0.634		0.000	0.540	0.560		0.000	1.476	2.543	
0.3	0.490	0.498	0.534		0.000	0.427	0.458		0.000	1.580	2.825	
0.4	0.405	0.414	0.452		0.000	0.367	0.397		0.000	2.004	3.625	
0.5	0.338	0.346	0.383		0.000	0.342	0.360		0.000	3.067	5.391	
0.6	0.281	0.286	0.321		0.000	0.341	0.335		0.000	5.735	9.378	
0.7	0.230	0.233	0.264		0.000	0.350	0.312		0.000	13.48	20.03	
0.8	0.179	0.181	0.210		0.000	0.355	0.285		0.000	44.82	59.96	
0.9	0.124	0.126	0.146		0.000	0.312	0.260		0.000	307.6	401.4	

$(1-\lambda)^3 F_{I,\lambda_1}/F_{I,\lambda_1}|_{\lambda\to 0}$ is for columns 2–5, $(1-\lambda)^3 F_{II,\lambda_2}/F_{II,\lambda_2}|_{\lambda\to 0}$ is for columns 6–9 and F_{III,λ_4} is for columns 10–13.

Acknowledgements

References

[1] Benthem JP, Koiter WT. In: Sih GC, editor. Mechanics of fracture 1. Noordhoff Int Pub 1, 1973:131–78.

[2] Nisitani H, Noda NA. Tension of a cylindrical bar having an infinite row of circumferential cracks. Engng Fract Mech 1984;20:678–86.

[3] Noda N-A, Takase Y, Chen MC. Generalized stress intensity factors in the interaction between two fibers in matrix. Int J Fract 2000;103:19–39.

[4] Chen DH, Nisitani H. Singular stress field near the corner of jointed dissimilar materials. Trans ASME, Ser E, J Appl Mech 1993;60:607–13.

[5] Chen DH, Nisitani H. Singular stress field near a corner of jointed dissimilar materials under antiplane loads. JSME Int J, Ser I 1992;35:399–403.

[6] Chen DH, Nisitani H. Analysis of intensity of singular stress field at fiber end (1st report, method of analysis). Trans Jpn Soc Mech Engng, Ser A 1992;58:1834–8 [in Japanese].

[7] Chen DH, Nisitani H. Analysis of intensity of singular stress field at fiber end (2nd report, results of calculation). Trans Jpn Soc Mech Engng, Ser A 1992;58:2153–8 [in Japanese].

[8] Bogy DB, Wang KC. Stress singularities at interface corners in bonded dissimilar isotropic elastic materials. Int J Solids Struct 1971;7:993–1008.

[9] Chen DH. Stress intensity factors for V-notched strip under tension or in-plane bending. Int J Fract 1995;70:81–97.

[10] Chen DH. Antiplane strain problem of diamond inclusion. Int J Fract 1995;71:197–212.

[11] Noda NA, Kawashima Y, Moriyama S, Oda K. Interaction of newly defined stress intensity factors for angular corners in a row of diamond-shaped inclusions. Int J Fract 1996;82:267–95.

[12] Chen DH, Iwanaga T. Interaction between fibers. In: Proceedings of the 71st JSME Fall Annual Meeting. 1993. p. 245–7 [in Japanese].

[13] Noda N-A, Wang Q, Morodomi T, Uemura Y. Analysis of newly defined stress intensity factors at the end of rectangular and cylindrical inclusions. Key Engng Mater 1998;145–149:77–82.

[14] Chen DH, Noda N-A, Takase Y, Morodomi T. Evaluation of static strength by the application of stress intensity of angular corner. Trans Jpn Soc Mech Engng, Ser A 1996;62:1445–9 [in Japanese].

[15] Chen DH, Noda N-A. A consideration on the fracture criterion for a sharp notch. Trans Jpn Soc Mech Engng, Ser A 1998;64:2574–82 [in Japanese].

[16] Noda N-A, Chen DH, Takase Y, Morodomi T. Evaluation of static strength by the application of mixed mode stress intensity of angular corner. Trans Jpn Soc Mech Engng, Ser A 1998;64:958–63 [in Japanese].

[17] Nisitani H, Noda N-A. Stress concentration of a cylindrical bar having a V-shaped circumferential groove under torsion, tension, or bending. Engng Fract Mech 1984;20:743–66.

[18] Noda N-A, Oda K, Inoue T. Analysis of newly-defined stress intensity factors for angular corners using singular integral equations of the body force method. Int J Fract 1996;76:243–61.